

<https://doi.org/10.1038/s42003-026-09513-1>

# Hepatic HMGCS2-derived $\beta$ -hydroxybutyrate attenuates hippocampal insulin resistance and neuroinflammation to promote MASLD-induced cognitive function

Check for updates

Lijuan Nie<sup>1,2,5</sup>, Jing Sun<sup>1,5</sup>, Weilong Xu<sup>1,5</sup>, Xinyi Yang<sup>1</sup>, Gaoxiang Wang<sup>1</sup>, Ying Wang<sup>3</sup>, Tao Jiang<sup>4</sup>, Yutian Cao<sup>1</sup>, Hao Chen<sup>1</sup>, Qingrong Xia<sup>2</sup> & Xiqiao Zhou<sup>1</sup>

Cognitive impairment is a known complication of metabolic dysfunction-associated steatotic liver disease (MASLD), and  $\beta$ -hydroxybutyrate (BHB), a ketone body providing alternative brain energy under metabolic stress, may exert neuroprotective effects. This study explored BHB's role in MASLD-related cognitive impairment and its underlying mechanisms using a 20-week high-fat diet (HFD)-induced MASLD mouse model with cognitive dysfunction, comparing 3-hydroxy-3-methylglutaryl-CoA synthase 2 (*Hmgcs2*) knockout (KO), wild-type (WT), and exogenous BHB-supplemented mice. Key outcomes included hippocampal pathology, neuroinflammation, insulin resistance, amyloid- $\beta$  (A $\beta$ ) deposition, tau phosphorylation, glucose/lipid homeostasis, and cognitive function. Results showed *Hmgcs2* KO mice exhibited worse metabolic dysregulation (elevated triglycerides, cholesterol, hepatic lipid accumulation, impaired glucose tolerance, increased insulin, reduced BHB), cognitive decline (confirmed by Y-maze and novel object recognition tests), hippocampal p-Tau/A $\beta$  aggregation, neuroinflammation (elevated iNOS, COX-2, IL-1 $\beta$ ), and impaired IRS/PI3K/AKT/GSK3 $\beta$  signaling, whereas exogenous BHB supplementation alleviated these phenotypes. Collectively, reduced *Hmgcs2* expression and BHB levels critically contribute to MASLD-induced cognitive impairment via cerebral insulin signaling disruption and neuroinflammation, highlighting BHB's therapeutic potential.

With rapid shifts in dietary patterns and lifestyles, the prevalence of metabolic dysfunction-associated steatotic liver disease (MASLD) is increasing annually, with a current global incidence of approximately 40% projected to rise to 55.7% by 2040<sup>1,2</sup>. The clinical burden of MASLD extends beyond liver-related morbidity and mortality, encompassing a range of extra-hepatic complications<sup>3</sup>. Recently, cognitive impairment has been recognized as a significant complication of MASLD<sup>4,5</sup>. Studies have shown that individuals with MASLD have more than double the risk of developing cognitive impairment compared to healthy controls<sup>6</sup>. These patients often experience

memory deficits and reduced attention, which can profoundly disrupt their daily functioning and overall quality of life<sup>7,8</sup>. Unfortunately, the precise mechanisms driving MASLD-induced cognitive impairment remain unclear, and effective therapeutic options are currently limited in clinical practice.

The hippocampus regulates cognitive functions, such as learning and memory, and is particularly vulnerable to environmental toxins, cardiovascular and metabolic dysregulation, as well as subsequent cognitive impairment<sup>9,10</sup>. Potential mechanisms linking metabolic disorders, such as

<sup>1</sup>Department of Endocrinology, Affiliated Hospital of Nanjing University of Chinese Medicine, Jiangsu Province Hospital of Chinese Medicine, Nanjing, China.

<sup>2</sup>Science and Education Department, Affiliated Psychological Hospital of Anhui Medical University, Hefei Fourth People's Hospital, Hefei, China. <sup>3</sup>Center for Health Management, Jiangsu Province Geriatric Hospital, Nanjing, China. <sup>4</sup>School of Pharmacy, Anhui Medical University, Hefei, China. <sup>5</sup>These authors contributed equally: Lijuan Nie, Jing Sun, Weilong Xu. e-mail: [ahmcxqr@163.com](mailto:ahmcxqr@163.com); [zhouxiqiao@njucm.edu.cn](mailto:zhouxiqiao@njucm.edu.cn)

MASLD, to cognitive decline include insulin resistance, inflammation, oxidative stress, disrupted glucose-energy homeostasis, gut dysbiosis, and vascular dysfunction, although the exact pathways remain unclear<sup>11–13</sup>. Inflammation and insulin resistance are common pathological mechanisms underlying both cognitive impairment and metabolic disorders, playing crucial roles in high-fat diet (HFD)-induced cognitive dysfunction<sup>14,15</sup>. Elevated neuroinflammation promotes serine phosphorylation of insulin receptor substrate-1 (IRS-1), disrupting hippocampal insulin signaling. This disturbance triggers Tau hyperphosphorylation and facilitates amyloid- $\beta$  (A $\beta$ ) deposition, ultimately contributing to cognitive decline<sup>14,15</sup>.

$\beta$ -Hydroxybutyrate (BHB), the primary ketone body in mammalian systems, is produced from fatty acid  $\beta$ -oxidation in the liver during fasting, prolonged physical exertion, and carbohydrate restriction. This metabolic byproduct is readily utilized by energy-demanding tissues, where it undergoes a two-step conversion: first to acetyl-CoA, then to ATP. This ATP acts as a vital energy source for essential organs such as the brain and heart<sup>16</sup>. The regulation of BHB synthesis is primarily influenced by two factors: the availability of fatty acids as precursors and the expression level and enzymatic activity of 3-hydroxy-3-methylglutaryl-CoA synthase 2 (HMGCS2)<sup>16</sup>. Preclinical and clinical studies have revealed that individuals with metabolic abnormalities, such as MASLD, and rodent models exhibit reduced blood ketone levels, accompanied by decreased HMGCS2 expression in the liver<sup>17–19</sup>. Moreover, enhancing Hmgcs2 expression or supplementing with BHB has been shown to significantly improve hepatic steatosis and glucose homeostasis<sup>20,21</sup>. Interestingly, HMGCS2 promotes the autophagy of A $\beta$  precursor proteins and Tau/p-Tau, thereby mitigating cognitive decline associated with Alzheimer's disease (AD) by modulating ketone body production<sup>22</sup>. Additionally, BHB supplementation has been demonstrated to benefit cognitive function by reducing A $\beta$  accumulation in the brain, attenuating excessive microglial activation, and improving mitochondrial respiratory function in hippocampal neurons<sup>23</sup>. Collectively, these findings highlight the potential significance of ketone bodies, particularly BHB, in both the pathophysiology and therapeutic strategies for MASLD and cognitive impairment. However, the role of the HMGCS2-BHB axis in MASLD-induced cognitive impairment remains poorly understood.

In this study, we established an HFD-induced MASLD model to systematically examine the effects of *Hmgcs2* knockout (KO) and exogenous BHB supplementation on cognitive function in mice, as well as their underlying molecular mechanisms.

## Results

### *Hmgcs2* deficiency exacerbates HFD-induced glucose and lipid metabolic disorders and cognitive impairment in mice

After 20 weeks of HFD feeding, both wild-type (WT) and *Hmgcs2* KO mice developed significant MASLD and cognitive impairment. As shown in Fig. 1, *Hmgcs2* KO mice exhibited accelerated weight gain (Fig. 1A) and more pronounced glucose intolerance compared to WT mice, evidenced by significantly increased area under the curve for the oral glucose tolerance test (AUC<sub>OGTT</sub>, Fig. 1B) and serum insulin (Fig. 1C) levels. Fasting blood glucose (FBG) levels were also elevated, though the increase did not reach statistical significance (Fig. 1D). *Hmgcs2* deficiency exacerbated HFD-induced hepatic lipid accumulation, as evidenced by elevated serum triglyceride (TG) and total cholesterol (TC) (Fig. 1E), an increased Non-alcoholic Steatohepatitis Activity Score (NAS) from hematoxylin and eosin (H&E) staining (Fig. 1F, G), and a greater percentage of lipid droplet area from Oil Red O staining (Fig. 1F, H). *Hmgcs2* deficiency did not affect HFD-induced liver fibrosis (Fig. 1F and Supplementary Fig. 1A), likely because the 20-week HFD regimen itself was insufficient to induce significant fibrosis.

Cognitive assessments using the Y-maze (Fig. 1I) and novel object recognition (NOR, Fig. 1J) tests revealed that *Hmgcs2* KO mice exhibited more cognitive dysfunction than their WT littermates. Furthermore, serum BHB levels were significantly lower in *Hmgcs2* KO mice compared to WT controls (Fig. 1K). These findings suggest that *Hmgcs2* deficiency aggravates HFD-induced glucose and lipid metabolic dysregulation, as well as cognitive impairment, which is accompanied by reduced circulating BHB levels.

### *Hmgcs2* deficiency exacerbates HFD-induced hippocampal inflammation and insulin resistance in mice

*Hmgcs2* deficiency significantly exacerbated the chronic HFD-induced pro-inflammatory response in the hippocampus, as demonstrated by the marked upregulation of inducible nitric oxide synthase (iNOS) and cyclooxygenase-2 (COX-2) in both immunofluorescence (Fig. 2A, B) and Western Blot analyses (Fig. 2C and Supplementary Fig. 1B). This effect was further confirmed by a significant increase in IL-1 $\beta$  levels (Fig. 2A–C, and Supplementary Fig. 1B). Additionally, *Hmgcs2* KO mice exhibited heightened activation of the nuclear factor kappa-B ((NF- $\kappa$ B)/NLR family pyrin domain containing 3 (NLRP3) inflammasome pathway, accompanied by increased hippocampal IL-18 protein levels (Fig. 2D and Supplementary Fig. 1B). Given that IRS-1 serine phosphorylation is a hallmark of insulin resistance, we next investigated whether *Hmgcs2* deficiency impacts IRS-1 activation. Compared to WT controls, *Hmgcs2* KO mice displayed significantly elevated hippocampal IRS-1 phosphorylation at Ser612/636 and Ser1101 (Fig. 2E, F), indicating exacerbation of HFD-induced hippocampal insulin resistance. To further evaluate downstream insulin signaling, we analyzed the phosphorylation status of the phosphatidylinositol 3-kinase (PI3K)/protein kinase B (AKT) pathway and its effector glycogen synthase kinase-3 $\beta$  (GSK3 $\beta$ ). Elevated phosphorylation of PI3K, AKT, and GSK3 $\beta$  was observed in the hippocampus of *Hmgcs2* KO mice (Fig. 2E, G). These findings collectively demonstrate that *Hmgcs2* deficiency exacerbates HFD-induced hippocampal inflammation and insulin resistance in MASLD mice.

### *Hmgcs2* deficiency exacerbates HFD-induced hippocampal A $\beta$ and Tau neurotoxicity in mice

*Hmgcs2* KO mice exhibited significant upregulation of hippocampal amyloid precursor protein (APP) and beta-site APP cleaving enzyme 1 (BACE1) expression, shown by Western Blot (Fig. 2H and Supplementary Fig. 1C). This upregulation led to a pathogenic A $\beta$  profile, characterized by increased A $\beta$ 42 deposition, decreased A $\beta$ 40 levels, and a higher A $\beta$ 42/A $\beta$ 40 ratio (Fig. 2I–K). In parallel, phosphorylated tau (p-Tau) in the hippocampus was also markedly enhanced as shown by Western Blot (Fig. 2L and Supplementary Fig. 1C). Immunohistochemical analysis further confirmed these findings at the tissue level, revealing elevated levels of hippocampal APP, BACE1, and p-Tau in *Hmgcs2*-deficient mice (Fig. 2M, N). These findings collectively suggest that *Hmgcs2* deficiency exacerbates the neurotoxic effects of A $\beta$  and p-Tau, contributing to worsened hippocampal pathology in MASLD mice.

### BHB alleviates HFD-induced systemic glucose-lipid metabolic disorders and cognitive impairment in mice

The results of this study demonstrate that *Hmgcs2* deficiency exacerbates cognitive impairment in HFD-induced MASLD mice. Given these findings, we explored the therapeutic potential of BHB, a key metabolite regulated by *Hmgcs2*, as it may help mitigate the metabolic and cognitive dysfunctions associated with MASLD. Experimental results demonstrated that BHB supplementation significantly reduced body weight in MASLD mice (Supplementary Fig. 2A). Analyses of oral glucose tolerance test (OGTT), insulin, and FBG levels revealed that BHB effectively enhanced glucose clearance and ameliorated systemic insulin resistance (Fig. 3A–D). Further investigation showed that BHB intervention markedly decreased serum TC levels (Fig. 3E), slightly decreased serum TG levels (Supplementary Fig. 2B), and alleviated hepatic lipid accumulation (Fig. 3F and Supplementary Fig. 2C, D).

Chronic BHB supplementation significantly ameliorated cognitive deficits across multiple behavioral domains. In the Morris water-maze (MWM) test, BHB-treated mice exhibited a significant increase in the number of platform crossings (Fig. 3G, H), indicating restored spatial memory. This recovery was further supported by increased time spent in the target quadrant and a greater swimming distance within it (Supplementary Fig. 2E, F). Furthermore, the enhanced spontaneous alternation rate in the Y-maze (Fig. 3I) demonstrated a reversal of working memory impairment. Similarly, in the NOR test, BHB administration led to a higher discrimination ratio for the novel object (Fig. 3J), reflecting improved recognition memory. These behavioral findings consistently demonstrate that

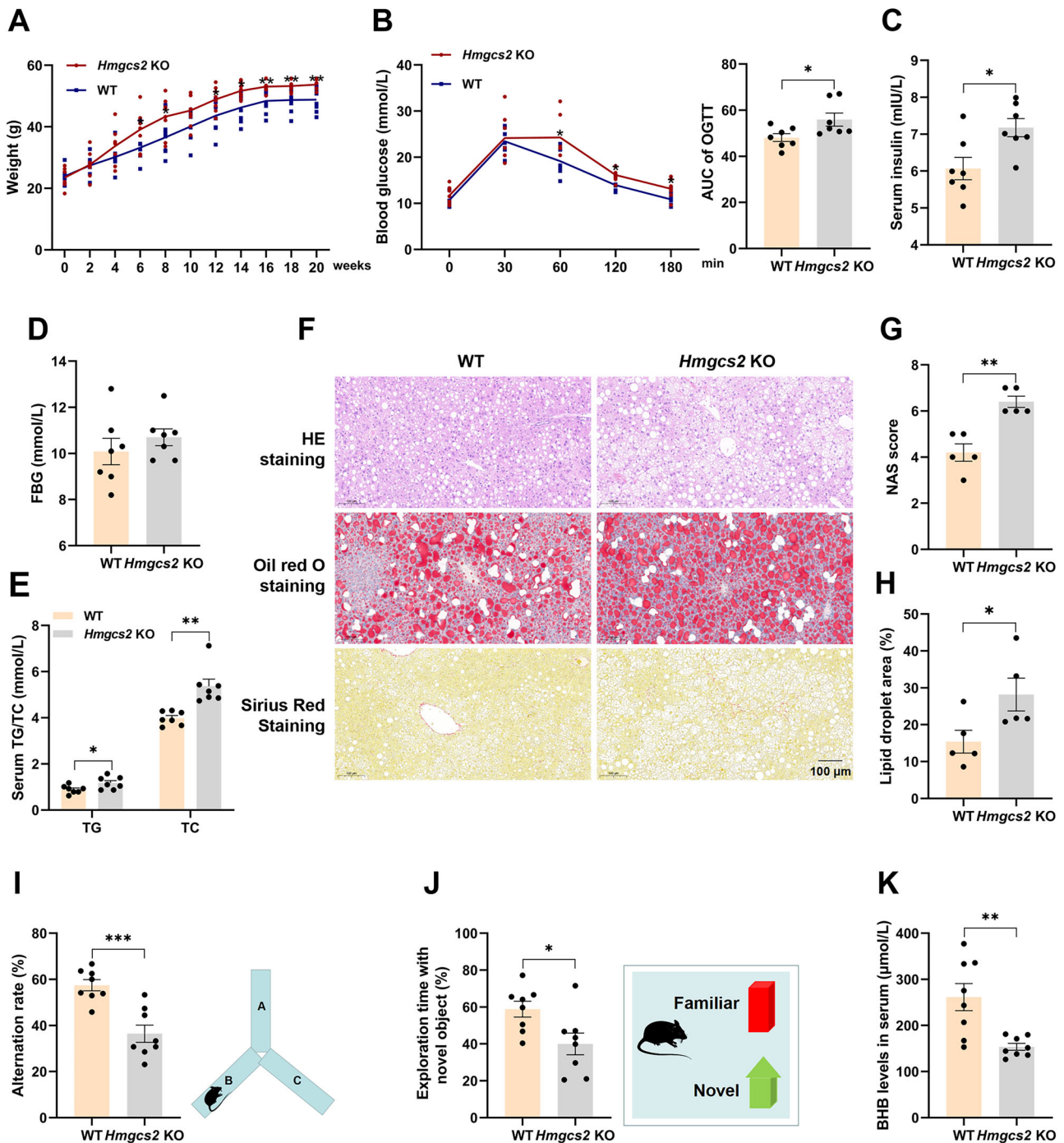
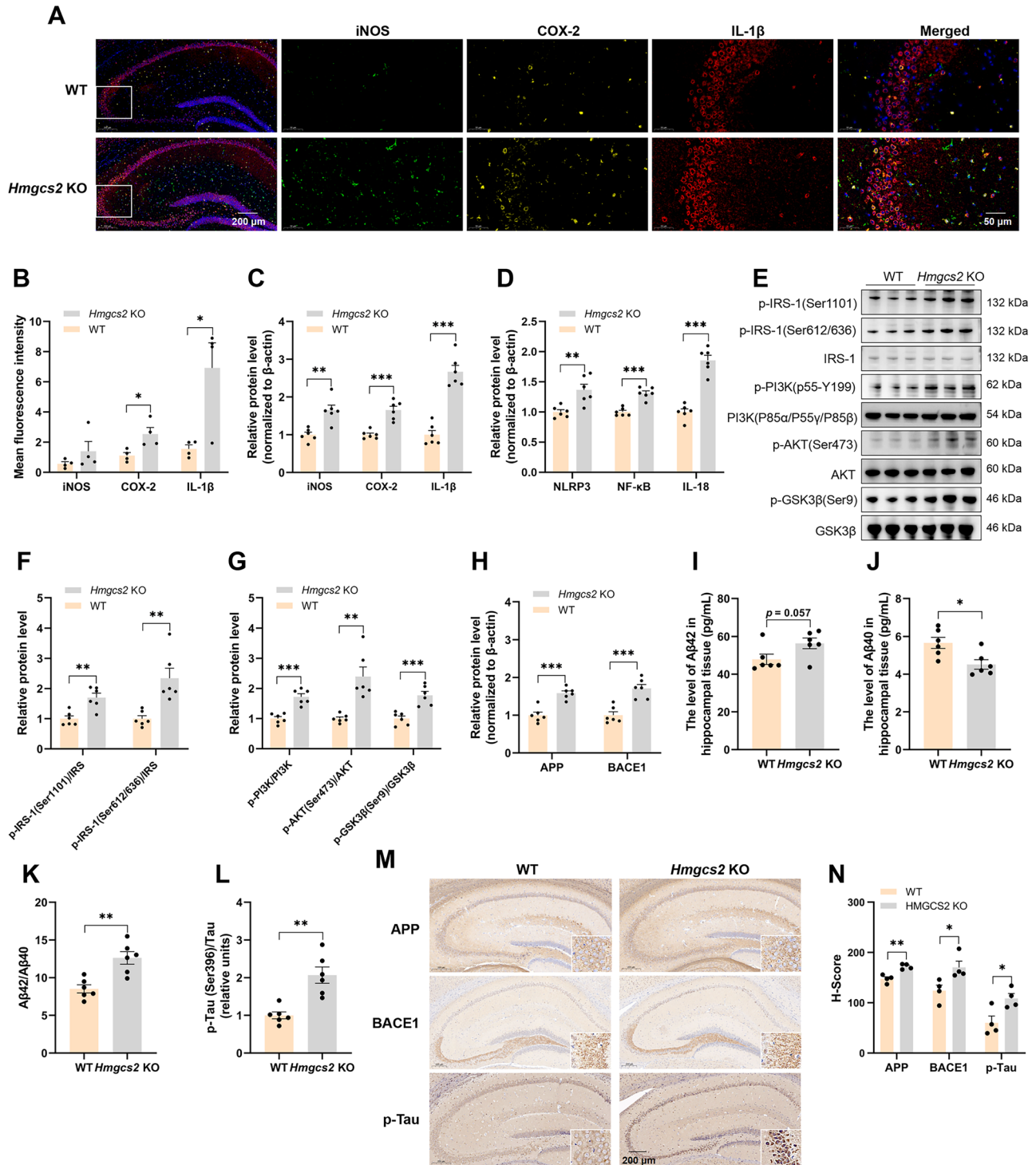


**Fig. 1 | *Hmgcs2* KO exacerbates metabolic disorders and cognitive impairment in HFD-fed mice.** **A** Body weight changes during the experimental period. 6 weeks:  $t = 2.163$ ,  $df = 14$ ,  $*p = 0.0484$ ; 8 weeks:  $t = 2.245$ ,  $df = 14$ ,  $*p = 0.0415$ ; 12 weeks:  $t = 2.232$ ,  $df = 14$ ,  $*p = 0.0425$ ; 14 weeks:  $t = 2.929$ ,  $df = 14$ ,  $*p = 0.0110$ ; 16 weeks:  $t = 3.014$ ,  $df = 14$ ,  $**p = 0.0093$ ; 18 weeks:  $t = 3.057$ ,  $df = 14$ ,  $**p = 0.0085$ ; 20 weeks:  $t = 3.359$ ,  $df = 14$ ,  $**p = 0.0047$ ;  $n = 8$  mice per group. **B** OGTT curves and the quantification of the area under the curve (AUC). 60 min:  $t = 2.530$ ,  $df = 12$ ,  $*p = 0.0264$ ; 120 min:  $t = 2.799$ ,  $df = 12$ ,  $*p = 0.0161$ ; 180 min:  $t = 2.341$ ,  $df = 12$ ,  $*p = 0.0373$ ; AUC:  $t = 2.361$ ,  $df = 12$ ,  $*p = 0.0360$ ;  $n = 7$  mice per group. **C** Fasting serum insulin levels.  $t = 2.835$ ,  $df = 12$ ,  $*p = 0.015$ ;  $n = 7$  mice per group. **D** FBG levels.  $t = 0.9060$ ,  $df = 12$ ,  $p = 0.383$ ;  $n = 7$  mice per group. **E** Serum TG and total cholesterol (TC) levels. TG:  $t = 2.297$ ,  $df = 12$ ,  $*p = 0.0404$ ; TC:  $t = 4.211$ ,  $df = 12$ ,  $**p = 0.0012$ ;  $n = 7$  mice per group. **F** Representative H&E, Oil Red O, and Sirius Red staining of liver tissue. Scale bar, 100 μm. **G** NAS calculated from H&E staining.  $t = 4.919$ ,  $df = 8$ ,  $**p = 0.0012$ ;  $n = 5$  mice per group. **H** Percentage of Oil Red O-stained area.  $t = 2.357$ ,  $df = 8$ ,  $*p = 0.0461$ ;  $n = 5$  mice per group. **I** Y-maze spontaneous alternation test and the corresponding diagram.  $t = 4.699$ ,  $df = 14$ ,  $***p < 0.001$ ;  $n = 8$  mice per group. **J** Percentage of exploration time with the novel object and schematic of the novel object recognition test.  $t = 2.589$ ,  $df = 14$ ,  $*p = 0.0214$ ;  $n = 8$  mice per group. **K** Serum BHB levels.  $t = 3.566$ ,  $df = 14$ ,  $**p = 0.0031$ ;  $n = 8$  mice per group. Error bars represent the standard error of the mean (SEM). Statistical comparisons were performed using unpaired two-tailed Student's *t*-test;  $*p < 0.05$ ,  $**p < 0.01$ ,  $***p < 0.001$ . WT wild-type, *Hmgcs2* 3-hydroxy-3-methylglutaryl-CoA synthase 2.



BHB intervention provides robust protection against HFD-induced cognitive dysfunction, encompassing short-term, long-term, and spatial memory domains.

Collectively, these findings suggest that chronic BHB supplementation provides comprehensive protection against HFD-induced systemic insulin resistance, glucose-lipid metabolic disorders, and cognitive dysfunction.

**BHB alleviates HFD-induced hippocampal neuronal damage and loss in mice**

Nissl staining was employed to evaluate neuronal loss and structural integrity. In the WT control group, the hippocampus displayed tightly packed

neurons with rounded nuclei, clear nucleoli, and abundant deep-purple Nissl bodies (Fig. 4A). In contrast, HFD-fed mice exhibited significant neuronal damage in the hippocampal cornu ammonis (CA) 1–3 regions, including neuronal loss (yellow arrows), disrupted architecture, nuclear pyknosis (red arrows), and a decrease in Nissl body density with pale staining (Fig. 4A–C). Following BHB treatment, there was a notable restoration of neuronal density, improved cellular morphology, and an increase in Nissl body content, as indicated by more intense purple staining (Fig. 4A–C). Similarly, H&E staining corroborated these findings, showing HFD-induced neuronal loss and nuclear pyknosis in CA1–3 regions, which were significantly improved by BHB treatment (Supplementary Fig. 3A).

**Fig. 2 | *Hmgcs2* KO exacerbates HFD-induced hippocampal neuroinflammation, insulin resistance, and neurotoxicity.** **A** Representative immunofluorescence images of inducible nitric oxide synthase (iNOS; green), COX-2 (yellow), and Interleukin-1 $\beta$  (IL-1 $\beta$ ; red) in the hippocampus of mice. Scale bar, 200  $\mu$ m, 50  $\mu$ m. **B** Mean fluorescence intensity of iNOS, COX-2, and IL-1 $\beta$ . iNOS:  $t = 1.258$ ,  $df = 6$ ,  $p = 0.2553$ ; COX-2:  $t = 2.983$ ,  $df = 6$ ,  $p = 0.0245$ ; IL-1 $\beta$ :  $t = 3.181$ ,  $df = 6$ ,  $p = 0.0191$ ;  $n = 4$  mice per group. **C** Quantification of iNOS, COX-2, and IL-1 $\beta$  protein levels by Western Blot. iNOS:  $t = 4.343$ ,  $df = 10$ ,  $p = 0.0015$ ; COX-2:  $t = 5.949$ ,  $df = 10$ ,  $p < 0.001$ ; IL-1 $\beta$ :  $t = 8.215$ ,  $df = 10$ ,  $p < 0.001$ ;  $n = 6$  mice per group. **D** Quantification of NLR family pyrin domain containing 3 (NLRP3), nuclear factor kappa-B (NF- $\kappa$ B), and IL-18 protein levels by Western Blot. NLRP3:  $t = 3.648$ ,  $df = 10$ ,  $p = 0.0045$ ; NF- $\kappa$ B:  $t = 6.624$ ,  $df = 10$ ,  $p < 0.001$ ; IL-1 $\beta$ :  $t = 8.790$ ,  $df = 10$ ,  $p < 0.001$ ;  $n = 6$  mice per group. **E–G** Western Blot analysis for phosphorylated IRS (Ser1101, Ser612/636), total IRS, phosphorylated PI3K (p55-Y199), total PI3K, phosphorylated AKT (Ser473), total AKT, phosphorylated GSK3 $\beta$  (Ser9), and total GSK3 $\beta$  in the hippocampus. p-IRS-1(Ser1101)/IRS:  $t = 4.058$ ,  $df = 10$ ,  $p = 0.0023$ ; p-IRS-1(Ser612/636)/IRS:  $t = 3.849$ ,  $df = 10$ ,  $p = 0.0032$ ; p-PI3K/PI3K:  $t = 5.896$ ,

$df = 10$ ,  $p < 0.001$ ; p-AKT(Ser473)/AKT:  $t = 4.377$ ,  $df = 10$ ,  $p = 0.0014$ ; p-GSK3 $\beta$ (Ser9)/GSK3 $\beta$ :  $t = 4.930$ ,  $df = 10$ ,  $p < 0.001$ ;  $n = 6$  mice per group. **H** Quantification of amyloid precursor protein (APP) and beta-site APP cleaving enzyme 1 (BACE1) protein levels by Western Blot. APP:  $t = 5.761$ ,  $df = 10$ ,  $p < 0.001$ ; BACE1:  $t = 5.139$ ,  $df = 10$ ,  $p < 0.001$ ;  $n = 6$  mice per group. **I, J** Quantification of hippocampal A $\beta$ 42 (**I**) and A $\beta$ 40 (**J**) levels by ELISA. A $\beta$ 42:  $t = 2.149$ ,  $df = 10$ ,  $p = 0.057$ ; A $\beta$ 40:  $t = 2.967$ ,  $df = 10$ ,  $p = 0.0141$ ;  $n = 6$  mice per group. **K** A $\beta$ 42/A $\beta$ 40 ratio.  $t = 4.142$ ,  $df = 10$ ,  $p = 0.0020$ ;  $n = 6$  mice per group. **L** Quantification of phosphorylated Tau (p-Tau; Ser396) /total Tau ratio by Western Blot.  $t = 4.540$ ,  $df = 10$ ,  $p = 0.0011$ ;  $n = 6$  mice per group. **M** Representative images of APP, BACE1, and p-Tau by immunohistochemistry. Scale bar, 200  $\mu$ m, 100  $\mu$ m. **N** Histochemistry score (H-Score) of APP, BACE1, and p-Tau. APP:  $t = 5.130$ ,  $df = 6$ ,  $p = 0.0022$ ; BACE1:  $t = 2.795$ ,  $df = 6$ ,  $p = 0.0314$ ; p-Tau:  $t = 2.917$ ,  $df = 6$ ,  $p = 0.0267$ ;  $n = 4$  mice per group. Error bars represent the SEM. Statistical comparisons were performed using unpaired two-tailed Student's  $t$ -test;  $^*p < 0.05$ ,  $^{**}p < 0.01$ ,  $^{***}p < 0.001$ . WT wild-type, *Hmgcs2* 3-hydroxy-3-methylglutaryl-CoA synthase 2.

These results highlight that BHB alleviates HFD-induced hippocampal neuronal damage and loss.

### BHB alleviates HFD-induced hippocampal inflammation

Our previous study showed that *Hmgcs2* deficiency exacerbates HFD-induced hippocampal inflammation (Fig. 2A–C). To further investigate hippocampal immune responses, we performed double immunofluorescence labeling for glial fibrillary acidic protein (GFAP; a reactive astrocyte marker) and ionized calcium-binding adapter molecule 1 (IBA1; a microglial activation marker). Compared to controls, HFD-fed mice displayed a significant increase in hippocampal GFAP-positive cells, and a non-significant increase in IBA1-positive cells (Fig. 4D–F). BHB treatment reduced the number of GFAP- and IBA1-positive cells, suggesting that BHB suppresses astrocyte and microglial activation. Activated microglia release potent pro-inflammatory cytokines such as IL-1 $\beta$ , COX-2, and iNOS. Consistent with this, immunofluorescence and Western Blot analysis revealed that the protein levels of IL-1 $\beta$ , iNOS, and COX-2 were elevated in the hippocampus of HFD-fed mice. Following treatment with BHB, these levels were significantly reduced (Fig. 5A–C and Supplementary Fig. 3B). These findings demonstrate that BHB alleviates HFD-induced hippocampal neuroinflammation.

### BHB alleviates HFD-induced hippocampal insulin resistance

Compared to control mice, HFD-fed mice showed significantly increased phosphorylation of IRS-1 at Ser612/Ser636 and Ser1101 in the hippocampus, indicating IRS-1 inactivation under HFD conditions, an effect that was reversed by BHB treatment (Fig. 5D, E). To further evaluate hippocampal insulin sensitivity, we assessed the phosphorylation status of PI3K/AKT and its downstream target, GSK3 $\beta$ , following insulin stimulation. HFD-fed mice exhibited elevated baseline phosphorylation of PI3K, AKT, and GSK3 $\beta$  in the hippocampus, which was suppressed by BHB treatment (Fig. 5D, F). These results suggest that BHB improves HFD-induced hippocampal insulin resistance.

### BHB inhibits HFD-induced hippocampal A $\beta$ formation and tau phosphorylation

BHB significantly reduced the protein expression of APP and BACE1 in the hippocampus of MASLD mice (Fig. 6A, B), along with a notable decrease in A $\beta$ 42 levels (Fig. 6C), a key pathological hallmark of AD. BHB had no significant effect on A $\beta$ 40 levels (Fig. 6D). However, it showed a non-significant trend toward reducing the A $\beta$ 42/A $\beta$ 40 ratio ( $p = 0.0948$ ) (Fig. 6E). Western Blot analysis revealed that BHB inhibited HFD-induced p-Tau in the hippocampus (Fig. 6F, G). Meanwhile, immunohistochemical analysis also revealed that BHB significantly reduced the levels of APP, BACE1, and p-Tau in the hippocampus of HFD-fed mice (Fig. 6H, I). These findings demonstrate that BHB mitigates the neurotoxic effects of A $\beta$  and p-Tau.

## Discussion

In this study, we established a MASLD mouse model by feeding mice an HFD for 20 weeks. Cognitive function was assessed using the Y-maze, NOR, and MWM tests. Our findings showed that *Hmgcs2* deficiency exacerbated HFD-induced systemic glucolipid dysregulation, insulin resistance, and cognitive dysfunction. However, supplementation with the metabolic product BHB significantly alleviated these pathological features in MASLD mice, primarily by reducing hippocampal inflammation, improving insulin sensitivity, and inhibiting the formation of A $\beta$  and p-Tau (Fig. 7).

In hepatic mitochondria, acetyl-CoA undergoes reactions catalyzed by HMGCS2, leading to the production of ketone bodies, such as acetoacetic acid, acetone, and BHB<sup>24</sup>. These ketones are used as alternative energy sources, especially by the brain<sup>16</sup>. The brain, being insulin-sensitive, needs proper insulin signaling for normal function. Insulin resistance is linked to metabolic diseases and AD<sup>25,26</sup>, and impaired signaling worsens AD's key features, Tau hyperphosphorylation and A $\beta$  accumulation<sup>26</sup>. Notably, BHB acts as an insulin sensitizer and plays a critical role in metabolic disorders like MASLD and type 2 diabetes<sup>27,28</sup>. We found that long-term HFD feeding specifically affects systemic glucose metabolism and leads to significant peripheral insulin resistance. This phenomenon is exacerbated by *Hmgcs2* KO and ameliorated by exogenous BHB supplementation. Unsurprisingly, HFD feeding also results in the disruption of the insulin-dependent IRS1-PI3K-AKT-GSK3 $\beta$  signaling pathway in the hippocampus. PI3K, AKT, and GSK3 $\beta$ , which are key kinases in the insulin signaling pathway, remained persistently in a marginally hyperphosphorylated state after HFD feeding and lost their responsiveness to insulin. Notably, as a central node in cellular signal transduction, GSK3 $\beta$  dysfunction triggers multiple pathological processes in the neurodegenerative brain, including cholinergic neuron and synaptic loss, A $\beta$  deposition, hyperphosphorylation of tau protein, and neuroinflammation<sup>15,29</sup>. In this study, BHB administration reduced serum insulin levels, improved glucose disposal in mice, and restored the IRS1-PI3K-AKT-GSK3 $\beta$  signaling pathway. These results show that BHB alleviated HFD-induced cognitive dysfunction by enhancing hippocampal insulin sensitivity.

Impaired insulin signaling is a key contributor to the two core pathological features of AD: tau hyperphosphorylation and A $\beta$  accumulation. Regarding tau pathology, we found that the HFD induced tau phosphorylation specifically at the Ser396 residue, a canonical AD epitope whose pathological relevance is well-established<sup>30</sup>. This modification was mechanistically linked to the activation of GSK-3 $\beta$ , the primary kinase responsible for this site<sup>31</sup>. These results suggest that HFD may contribute to AD pathogenesis by triggering early-stage disease mechanisms. The administration of BHB effectively suppressed GSK-3 $\beta$  activity, thereby reducing this specific pathogenic tau phosphorylation and disrupting a critical cascade leading to neurodegeneration. Furthermore, the selective reduction of A $\beta$ 42—without proportional effects on A $\beta$ 40—suggests a potential mechanism involving enhanced  $\gamma$ -secretase processivity<sup>32,33</sup>. This

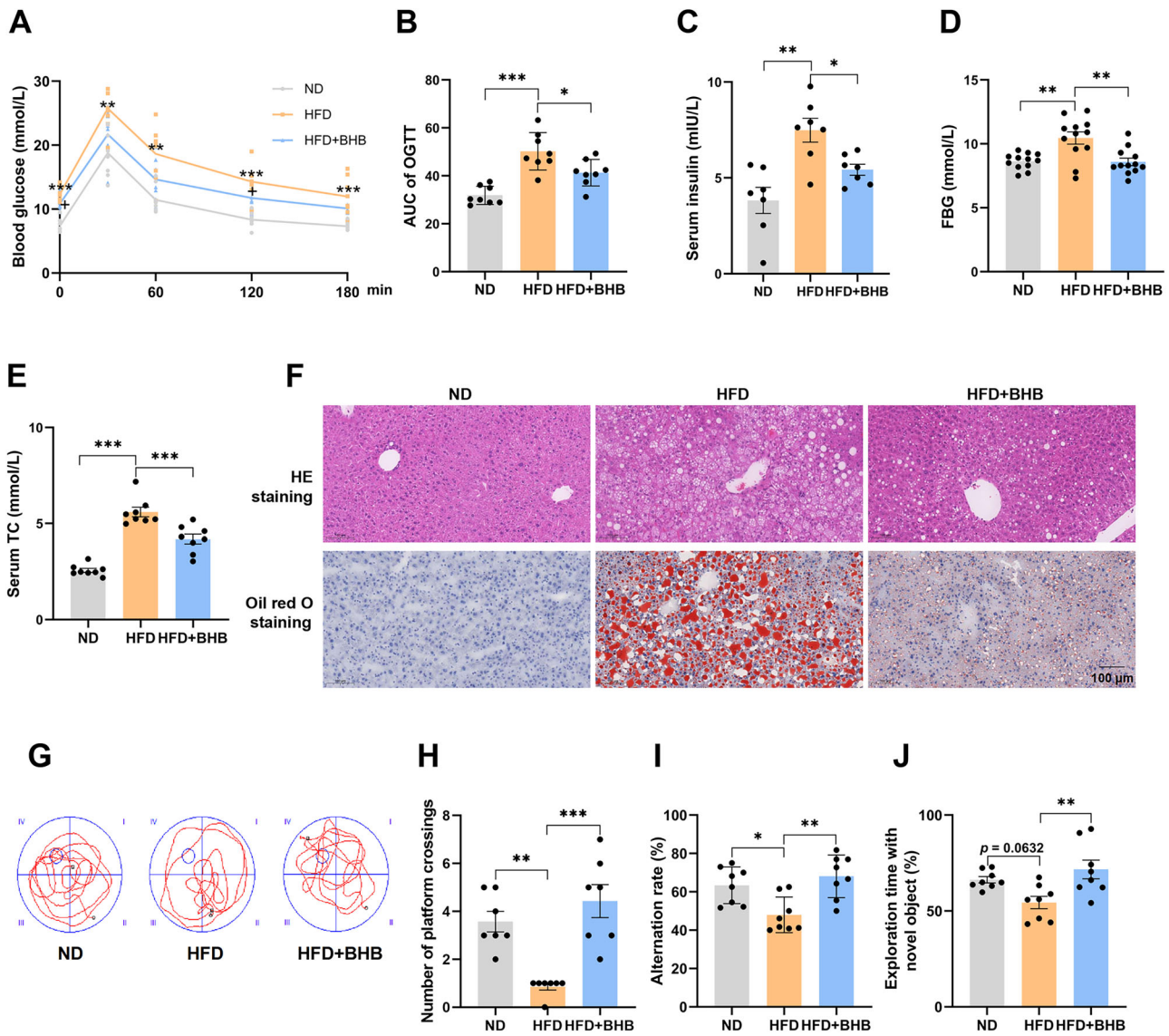


**Fig. 3 | BHB ameliorates HFD-induced systemic glucose/lipid metabolic disturbances, insulin resistance, and cognitive dysfunction in mice.** **A, B** OGTT curves and the quantification of the area under the curve (AUC). 0 min: F (2, 21) = 37.84, ND vs HFD:  $***p < 0.001$ , HFD vs HFD + BHB:  $^+p = 0.0451$ ; 30 min: F (2, 21) = 7.175, ND vs HFD:  $**p = 0.0031$ , HFD vs HFD + BHB:  $p = 0.0949$ ; 60 min: F (2, 21) = 9.434, ND vs HFD:  $***p < 0.001$ , HFD vs HFD + BHB:  $p = 0.0610$ ; 120 min: F (2, 21) = 18.66, ND vs HFD:  $***p < 0.001$ , HFD vs HFD + BHB:  $^+p = 0.0410$ ; 180 min: F (2, 21) = 13.31, ND vs HFD:  $***p < 0.001$ , HFD vs HFD + BHB:  $p = 0.1243$ ; AUC: F (2, 21) = 19.16, ND vs HFD:  $***p < 0.001$ , HFD vs HFD + BHB:  $^+p = 0.0180$ ;  $n = 8$  mice per group. **C** Fasting serum insulin levels. F (2, 18) = 10.88, ND vs HFD:  $***p < 0.001$ , HFD vs HFD + BHB:  $^+p = 0.0438$ ;  $n = 7$  mice per group. **D** FBG levels. F (2, 33) = 10.03, ND vs HFD:  $**p = 0.0015$ , HFD vs HFD + BHB:  $**p = 0.0012$ ;  $n = 12$  mice per group. **E** Serum total cholesterol (TC) levels. F (2, 21) = 50.38, ND vs HFD:  $***p < 0.001$ , HFD vs HFD + BHB:  $***p < 0.001$ ;  $n = 8$  mice per group. **F** Representative H&E and Oil Red O staining of liver tissue.  $n = 5$  mice per group. Scale bar, 100  $\mu\text{m}$ . **G** Representative swimming paths in the Morris water-maze (MWM) test. **H** Platform crossings in the MWM test. F (2, 18) = 15.48, ND vs HFD:  $**p = 0.0021$ , HFD vs HFD + BHB:  $***p < 0.001$ ;  $n = 7$  mice per group. **I** Spontaneous alternation percentage in the Y-Maze test. F (2, 21) = 8.838, ND vs HFD:  $^+p = 0.0151$ , HFD vs HFD + BHB:  $**p = 0.0017$ ;  $n = 8$  mice per group. **J** Novel object exploration time in the novel object recognition test. F (2, 21) = 6.404, ND vs HFD:  $p = 0.0632$ , HFD vs HFD + BHB:  $**p = 0.0058$ ;  $n = 8$  mice per group. Error bars represent the SEM. Statistical comparisons were performed using One-way ANOVA with Tukey's post hoc test;  $^+p < 0.05$ ,  $**p < 0.01$ ,  $***p < 0.001$ . ND normal diet, BHB  $\beta$ -hydroxybutyrate, HFD high-fat diet.

shift in cleavage preference toward shorter, less amyloidogenic A $\beta$  species (e.g., A $\beta$ 38 and A $\beta$ 40) would effectively lower the A $\beta$ 42/A $\beta$ 40 ratio, a key AD pathological hallmark, and aligns with the action of known  $\gamma$ -secretase modulators<sup>33,34</sup>. Certainly, this is merely an experimental hypothesis, and further experiments are required for its verification.

Inflammation is a key pathological link connecting MASLD and cognitive impairment<sup>35</sup>. Chronic low-grade inflammation is a characteristic feature of MASLD pathogenesis, with inflammation initially confined to the liver. Pro-inflammatory cytokines (e.g., IL-6, IL-1 $\beta$ , and TNF- $\alpha$ ) released by the liver trigger systemic inflammation, disrupt the blood-brain barrier, and activate microglia and astrocytes in the central nervous system<sup>35,36</sup>. Activated

glial cells amplify neuroinflammation by increasing the expression of COX-2 and iNOS while releasing additional cytokines (e.g., IL-6, IL-1 $\beta$ , and TNF- $\alpha$ )<sup>37</sup>. This forms a self-perpetuating vicious cycle of persistent glial cell activation and escalating neuroinflammation. Enhanced neuroinflammation promotes serine phosphorylation of IRS-1 and impairs insulin signaling in the hippocampus<sup>38</sup>. Additionally, persistent glial cell-mediated neuroinflammation exacerbates oxidative stress through multiple mechanisms<sup>39,40</sup>, and these mechanisms collectively contribute to a neurotoxic environment that promotes A $\beta$  formation and tau hyperphosphorylation. In this study, BHB treatment significantly reduced the reactive upregulation of HFD-induced glial cells and simultaneously decreased the levels of iNOS, COX-2,

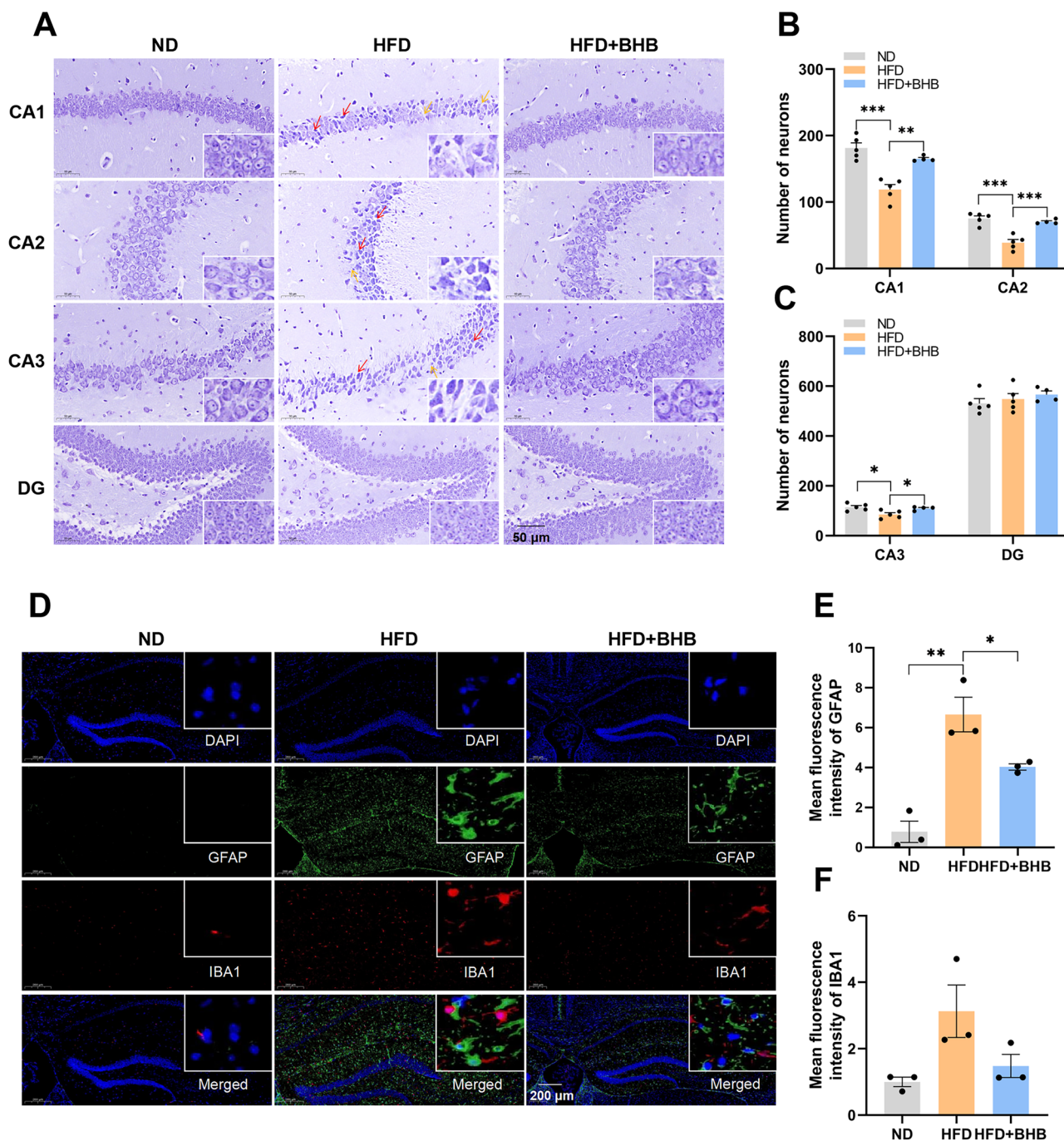


**Fig. 4 | BHB ameliorates HFD-induced hippocampal neuronal damage and neuroinflammation in mice.** **A** Representative diagram of Nissl staining. Scale bar, 50  $\mu$ m. **B, C** Neuronal density in hippocampal cornu ammonis (CA)1, CA2, CA3, and dentate gyrus (DG) regions. CA1: F (2, 11) = 24.60, ND vs HFD:  $***p < 0.001$ , HFD vs HFD + BHB:  $**p = 0.0016$ ; CA2: F (2, 11) = 26.95, ND vs HFD:  $***p < 0.001$ , HFD vs HFD + BHB:  $***p < 0.001$ ; CA3: F (2, 11) = 7.444, ND vs HFD:  $*p = 0.0110$ , HFD vs HFD + BHB:  $*p = 0.0426$ ; DG: F (2, 11) = 0.7730, ND vs HFD:  $p = 0.8086$ , HFD vs HFD + BHB:  $p = 0.7956$ ;  $n = 5$  mice for ND and HFD group,  $n = 4$  mice for HFD + BHB group. **D** Representative immunofluorescence images of glial fibrillary acidic protein (GFAP; green) and ionized calcium-binding adapter molecule 1

(IBA1; red) in the hippocampus of mice. Scale bar, 200  $\mu$ m, 50  $\mu$ m. **E, F** Mean fluorescence intensity of GFAP and IBA1. GFAP: F (2, 6) = 24.52, ND vs HFD:  $**p = 0.0010$ , HFD vs HFD + BHB:  $*p = 0.0465$ ; IBA1: F (2, 6) = 4.886, ND vs HFD:  $p = 0.0558$ , HFD vs HFD + BHB:  $p = 0.1304$ ;  $n = 3$  mice per group. The red arrows indicate nuclear pyknosis (condensed chromatin) and morphological alterations; yellow arrows denote neuronal loss and disorganized cellular arrangement. Error bars represent the SEM. Statistical comparisons were performed using One-way ANOVA with Tukey's post hoc test;  $*p < 0.05$ ,  $**p < 0.01$ ,  $***p < 0.001$ . BHB  $\beta$ -hydroxybutyrate, HFD high-fat diet, ND normal diet.

and IL-1 $\beta$ , thereby protecting the hippocampal region of HFD-fed mice from inflammatory damage. Mechanistically, BHB primarily reduces the release of pro-inflammatory cytokines by inhibiting the activity of the NLRP3 inflammasome and regulating epigenetic modifications<sup>41,42</sup>. This explains the observed resolution of neuroinflammation in this study.

The exact cause of MASLD is not fully understood, but recent studies suggest that impaired ketogenesis may play a key role. Research shows that disrupted ketone production speeds up MASLD progression<sup>43,44</sup>. Notably, patients with metabolic dysfunction-associated steatohepatitis have lower *Hmgcs2* expression compared to those with MASLD<sup>45</sup>. Additionally, both

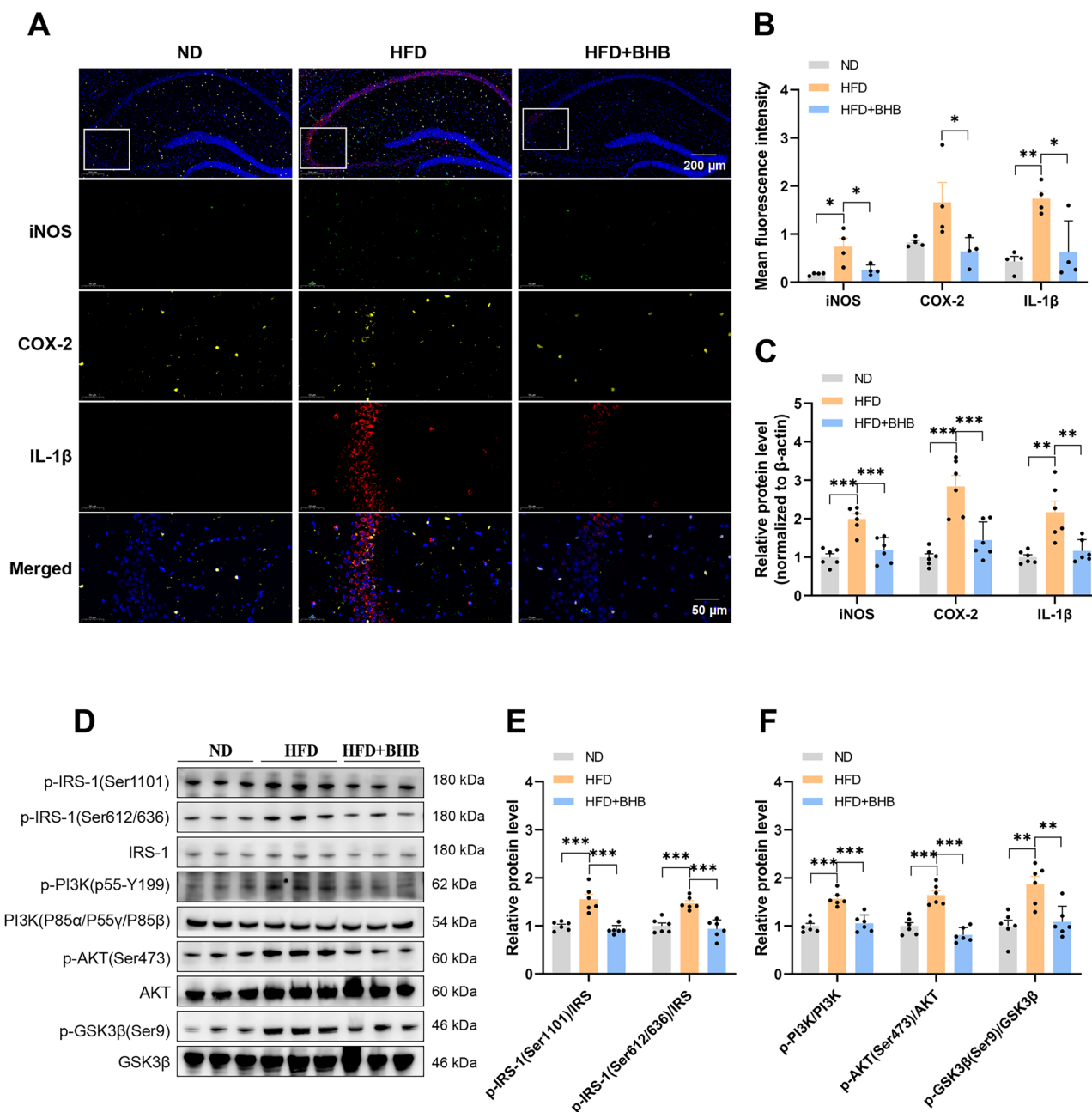


**Fig. 5 | BHB ameliorates HFD-induced hippocampal neuroinflammation and insulin resistance in mice.** **A** Representative immunofluorescence images of inducible nitric oxide synthase (iNOS; green), COX-2 (yellow), and Interleukin-1 $\beta$  (IL-1 $\beta$ ; red) in the hippocampus of mice. Scale bar, 200  $\mu$ m, 50  $\mu$ m. **B** Mean fluorescence intensity of iNOS, COX-2, and IL-1 $\beta$ . iNOS: F (2, 9) = 8.109, ND vs HFD:  $^*p = 0.0120$ , HFD vs HFD + BHB:  $^*p = 0.0266$ ; COX-2: F (2, 9) = 4.509, ND vs HFD:  $p = 0.1060$ , HFD vs HFD + BHB:  $^*p = 0.0480$ ; IL-1 $\beta$ : F (2, 9) = 10.36, ND vs HFD:  $^{**}p = 0.0058$ , HFD vs HFD + BHB:  $^*p = 0.0143$ ;  $n = 4$  mice per group. **C** Quantification of iNOS, COX-2, and IL-1 $\beta$  protein levels by Western Blot. iNOS: F (2, 15) = 19.54, ND vs HFD:  $^{***}p < 0.001$ , HFD vs HFD + BHB:  $^{***}p < 0.001$ ; COX-2: F (2, 15) = 21.49, ND vs HFD:  $^{***}p < 0.001$ , HFD vs HFD + BHB:  $^{***}p < 0.001$ ; IL-1 $\beta$ : F (2, 15) = 11.72, ND vs HFD:  $^{**}p = 0.0012$ , HFD vs HFD + BHB:  $^{**}p = 0.0042$ ;  $n = 6$  mice per group. **D–F** Western Blot analysis for phosphorylated IRS (Ser1101,

Ser612/636), total IRS, phosphorylated PI3K (p55-Y199), total PI3K, phosphorylated AKT (Ser473), total AKT, phosphorylated GSK3 $\beta$  (Ser9), and total GSK3 $\beta$  in the hippocampus. p-IRS-1(Ser1101)/IRS: F (2, 15) = 26.13, ND vs HFD:  $^{***}p < 0.001$ , HFD vs HFD + BHB:  $^{***}p < 0.001$ ; p-IRS-1(Ser612/636)/IRS: F (2, 15) = 20.26, ND vs HFD:  $^{***}p < 0.001$ , HFD vs HFD + BHB:  $^{***}p < 0.001$ ; p-PI3K/PI3K: F (2, 15) = 24.19, ND vs HFD:  $^{***}p < 0.001$ , HFD vs HFD + BHB:  $^{***}p < 0.001$ ; p-AKT(-Ser473)/AKT: F (2, 15) = 34.37, ND vs HFD:  $^{***}p < 0.001$ , HFD vs HFD + BHB:  $^{***}p < 0.001$ ; p-GSK3 $\beta$ (Ser9)/GSK3 $\beta$ : F (2, 15) = 11.52, ND vs HFD:  $^{**}p = 0.0015$ , HFD vs HFD + BHB:  $^{**}p = 0.0037$ ;  $n = 6$  mice per group. Error bars represent the SEM. Statistical comparisons were performed using One-way ANOVA with Tukey's post hoc test;  $^*p < 0.05$ ,  $^{**}p < 0.01$ ,  $^{***}p < 0.001$ . BHB  $\beta$ -hydroxybutyrate, HFD high-fat diet, ND normal diet.

MASLD patients and rodent models have reduced BHB levels<sup>17,19</sup>. BHB, a water-soluble ketone, can cross the blood-brain barrier and provide energy to the brain during low-glucose conditions<sup>46</sup>. Studies have shown BHB's potential to improve cognitive function through various mechanisms<sup>23,47,48</sup>. The HMGCS2-BHB axis serves as a potential bridge linking MASLD and

cognitive dysfunction. In this study, compared to the WT MASLD mice, *Hmgcs2* KO mice exhibited a significant metabolic dysregulation phenotype, characterized by elevated serum TG and cholesterol levels, exacerbated hepatic lipid accumulation, and impaired glucose tolerance. Additionally, *Hmgcs2* KO mice displayed increased circulating insulin levels and reduced

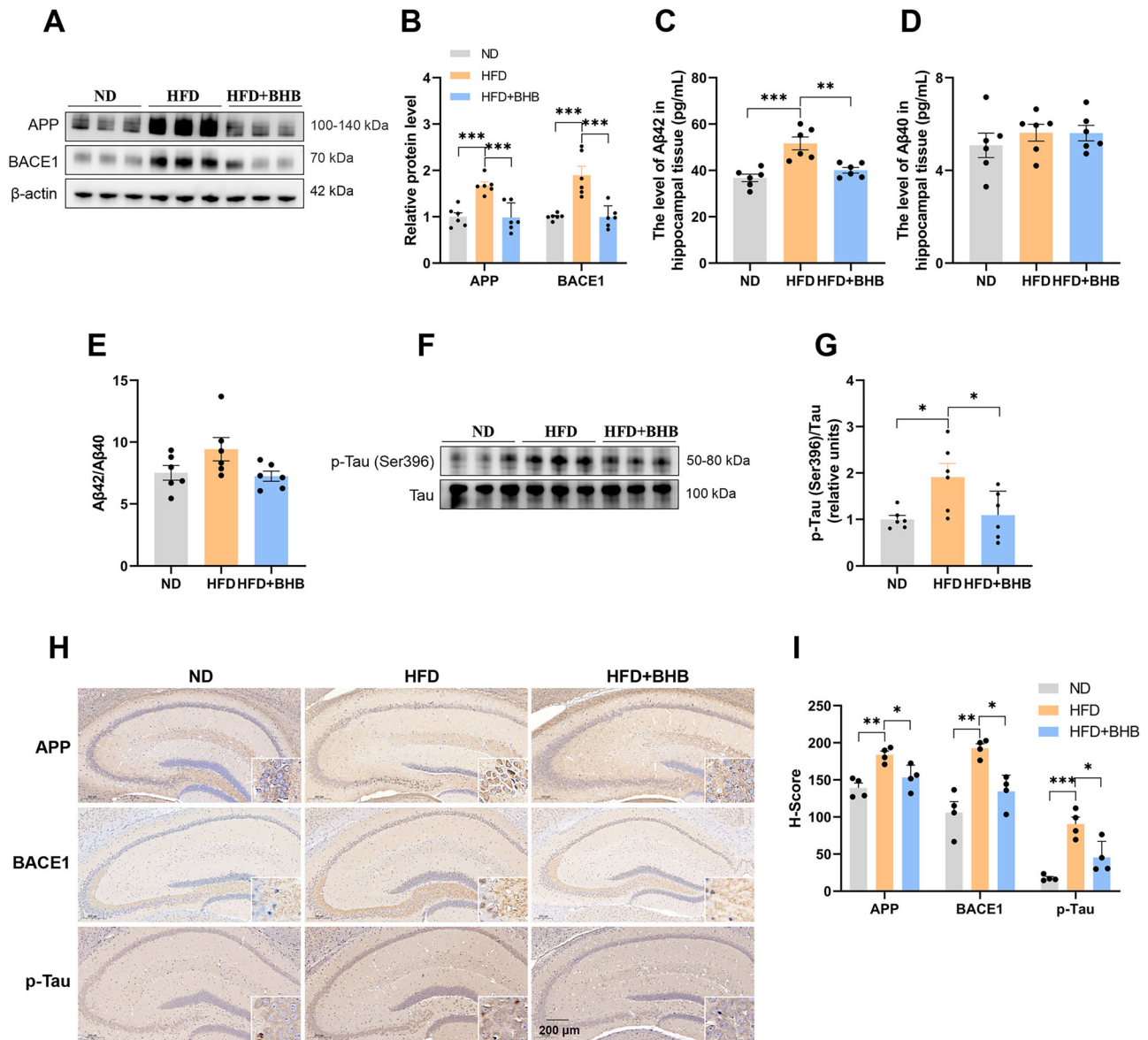


**Fig. 6 | BHB ameliorates HFD-induced hippocampal neurotoxicity.** **A, B** Western Blot analysis for APP and BACE1. APP: F (2, 15) = 16.04, ND vs HFD: \*\*\**p* < 0.001, HFD vs HFD + BHB: \*\*\**p* < 0.001; BACE1: F (2, 15) = 17.26, ND vs HFD: \*\*\**p* < 0.001, HFD vs HFD + BHB: \*\*\**p* < 0.001; *n* = 6 mice per group. **C, D** Quantification of hippocampal Aβ42 (**C**) and Aβ40 (**D**) levels by ELISA. Aβ42: F (2, 15) = 15.46, ND vs HFD: \*\*\**p* < 0.001, HFD vs HFD + BHB: \*\**p* = 0.0025; Aβ40: F (2, 15) = 0.5499, ND vs HFD: *p* = 0.6372, HFD vs HFD + BHB: *p* = 0.9997; *n* = 6 mice per group. **E** Aβ42/Aβ40 ratio. F (2, 15) = 3.006, ND vs HFD: *p* = 0.1543, HFD vs HFD + BHB: *p* = 0.0948; *n* = 6 mice per group. **F, G** Western Blot analysis for phosphorylated Tau (p-Tau; Ser396) and total Tau. F (2, 15) = 5.500, ND vs HFD:

\**p* = 0.0224, HFD vs HFD + BHB: \**p* = 0.0406; *n* = 6 mice per group. **H** Representative images of APP, BACE1, and p-Tau by immunohistochemistry. Scale bar, 200 μm, 100 μm. **I** Histochemistry score (H-Score) of APP, BACE1, and p-Tau. APP: F (2, 9) = 11.20, ND vs HFD: \*\**p* = 0.0032, HFD vs HFD + BHB: \**p* = 0.0272; BACE1: F (2, 9) = 15.90, ND vs HFD: \*\**p* = 0.0010, HFD vs HFD + BHB: \**p* = 0.0119; p-Tau: F (2, 9) = 19.38, ND vs HFD: \*\*\**p* < 0.001, HFD vs HFD + BHB: \**p* = 0.0104; *n* = 4 mice per group. Error bars represent the SEM. Statistical comparisons were performed using One-way ANOVA with Tukey's post hoc test; \**p* < 0.05, \*\**p* < 0.01, \*\*\**p* < 0.001. BHB β-hydroxybutyrate, HFD high-fat diet, ND normal diet.

BHB levels. Cognitive behavioral tests confirmed a more pronounced decline in cognitive function in *Hmgcs2* KO MASLD mice. Conversely, exogenous BHB supplementation significantly improved disorders of glucose and lipid metabolism and cognitive dysfunction in MASLD mice. These data further confirm that the HMGCS2-BHB axis is a central mediator linking liver metabolic dysfunction to neurodegeneration in MASLD.

Despite the promising insights into the HMGCS2-BHB axis, our study has several limitations that guide future research. A primary gap is the lack of a BHB rescue experiment in *Hmgcs2* KO mice, which we identify as a foremost priority for future work. Furthermore, our therapeutic intervention requires optimization; we did not measure BHB concentrations, precluding a direct comparison with physiological ketosis achieved via dietary

interventions, while the dose-response relationship and long-term safety of supplementation remain undefined. The translational relevance is also constrained by our use of only male mice and the inherent limitations of the HFD model in fully recapitulating human disease complexity. Future studies should also investigate the potential contributions of other ketone bodies, such as acetoacetate. Addressing these points and ultimately validating our findings in human clinical trials will be crucial steps toward establishing BHB as a viable therapy for cognitive decline associated with metabolic disorders.

In conclusion, our findings suggest that *Hmgcs2* deficiency and decreased circulating BHB levels may represent a shared pathological basis for MASLD and its associated cognitive dysfunction. As a key metabolic

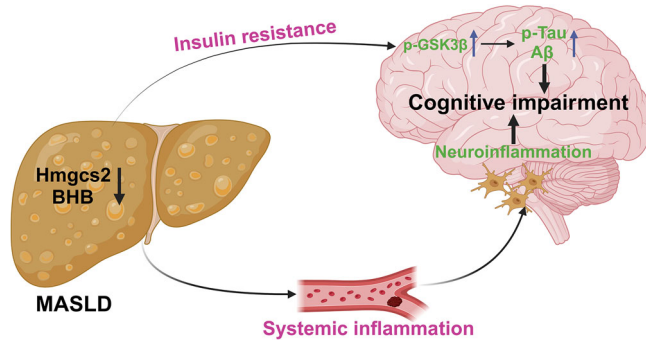


**Fig. 7 | The role and mechanisms of HMGCS2 and BHB in MASLD-induced cognitive impairment.** Initially, during the progression of MASLD, the downregulation of hepatic 3-hydroxy-3-methylglutaryl-CoA synthase 2 (HMGCS2) expression leads to reduced circulating BHB levels. By inducing hippocampal insulin resistance and neuroinflammatory responses, this metabolic disturbance subsequently promotes the pathological deposition of A $\beta$  and phosphorylated Tau (p-Tau), ultimately resulting in cognitive impairment.

regulator, BHB emerges as a promising therapeutic target for MASLD-related cognitive impairment. The neuroprotective mechanisms likely involve reducing peripheral and central insulin resistance and modulating neuroinflammatory pathways to offer cerebroprotective effects.

## Materials and methods

### Materials and reagents

The assay kits for total cholesterol (TC, #A111-1-1) and TG (#A110-1-1) were purchased from Nanjing Jiancheng Bioengineering Institute (Nanjing, China). The A $\beta$ 40 (#AF43246-A), A $\beta$ 42 (#AF43247-A), and insulin (#AF2579-A) ELISA kits were purchased from Aifang Biological Co., Ltd. (Changsha, China). The BHB (#RXJ99926) ELISA kit was purchased from Ruixin Biotech Co., Ltd. (Quanzhou, China). Sodium 3-hydroxybutyrate (#S27521) was purchased from Shanghai Yuanye Bio-Technology Co., Ltd. (Shanghai, China). The HFD formulated with 60% fat, 20% protein, and 20% carbohydrate was procured from Research Diets, Inc. (#D12492, New Brunswick, NJ, USA). Other reagents were obtained from Servicebio (Wuhan, China). The details of antibodies are shown in Supplementary Table 1.

### Animals and model establishment

*Hmgcs2* KO mice were generated by intercrossing heterozygous breeders (Strain ID: T004234; Strain Type: Cas9; Genetic Background: C57BL/6JGpt; GemPharmatech Co., Ltd., Nanjing, China). Genotypes were confirmed through PCR-based tail DNA analysis and Western blotting to verify protein depletion (Supplementary Fig. 4A, B). Age-matched male *Hmgcs2* KO mice ( $n = 12$ ) and wild-type (WT) littermate controls (8 weeks old,  $n = 12$ ) were subjected to a 20-week HFD regimen under standardized housing conditions. Male C57BL/6J mice (6 weeks old) were purchased from GemPharmatech Co., Ltd. (Nanjing, China) and housed under specific pathogen-free conditions with a 12-h light/dark cycle. After a 1-week acclimatization period, the mice were randomly assigned to two groups: normal diet (ND,  $n = 12$ ) and HFD ( $n = 24$ ). The mice were fed an HFD for a total of 20 weeks. After 8 weeks of HFD feeding, the HFD-fed mice were further divided into two subgroups: the BHB treatment group (BHB + HFD,  $n = 12$ ) and the HFD control group ( $n = 12$ ). Based on literature evidence<sup>46,49</sup>, mice in the BHB + HFD group were administered sodium 3-hydroxybutyrate (BHB) via intraperitoneal injection at a dose of 500 mg/kg body weight daily for 12 weeks, while the HFD control group received an equivalent volume of sterile phosphate-buffered saline (PBS).

At the conclusion of the study, mice were anesthetized with isoflurane at a flow rate of 300–500 ml/min. Euthanasia was then performed by cardiac puncture for blood collection. Subsequently, cardiac perfusion was performed. For tissues intended for biochemical or molecular analysis, mice

were perfused with cold PBS to clear the blood, after which the liver and brain tissues were harvested. For mice designated for histopathological examination, following the PBS perfusion, a subsequent perfusion with 4% paraformaldehyde was conducted for tissue fixation. We have complied with all relevant ethical regulations for animal use. The detailed protocols were approved by the Ethics Committee of Nanjing University of Chinese Medicine (approval no. 202211A037).

### OGTT

After a 12-h fasting period with free access to water, mice were administered an oral gavage of glucose (2.0 g/kg body weight, dissolved in sterile PBS). Blood samples were carefully collected via tail vein puncture at baseline (0 min) and at 30, 60, 120, and 180 min post-gavage using a glucometer. The area under the curve of the OGTT was then calculated based on the collected data.

### MWM test

The MWM test was conducted to assess spatial learning and memory in mice, following established protocols<sup>15</sup>. A circular pool (100 cm in diameter, with water temperature maintained at  $23 \pm 1$  °C) was divided into four quadrants, with a hidden platform (10 cm in diameter) placed 30 cm from the wall in quadrant IV. The experimental phases included: 1) visible platform training (Day 1, visual cue orientation); 2) hidden platform acquisition (Days 2–5, 4 trials per day with 30-min inter-trial intervals); and 3) probe trial (Day 6, platform removed). Each trial ended when the mouse mounted the platform ( $\geq 3$  s retention) or after 60 s, with guided platform exposure for 10 s if the mouse failed to find the platform. Spatial memory was quantified by the time spent in the target quadrant, the frequency of platform crossings, and path efficiency.

### NOR test

The NOR test was used to assess episodic memory in mice, utilizing their natural inclination to explore novel objects. The apparatus consisted of a white polyvinyl open-field arena ( $40 \times 40 \times 40$  cm) with three objects: two identical red cuboids (familiar objects, 10 cm in height) and a green polyagonal prism (novel object, height-matched to the cuboids). The protocol involved three phases: (1) Habituation (Day 1: 5 min of free exploration); (2) familiarization (Day 2: 10 min of exposure to two identical objects positioned 7 cm from the walls); and (3) testing (Day 3: 5 min of exploration with one novel and one familiar object). Inter-trial cleaning with 75% ethanol was strictly performed. Exploration time spent by the mice with the familiar and novel objects was recorded and analyzed statistically.

### Y-maze spontaneous alternation test

The Y-maze test was used to assess spatial working memory in mice. The maze consisted of three identical arms ( $30 \times 6 \times 15$  cm) radiating at 120° from a central area. Mice were placed in the central zone and allowed to explore freely for 8 min. Arm entries were recorded using video analysis. A valid alternation was defined as three consecutive entries into different arms, with the maximum possible alternations calculated as (total arm entries – 2). The alternation rate was expressed as a percentage, calculated using the formula: (actual alternations/maximum possible alternations)  $\times$  100.

### ELISA measurements and biochemical assays

Serum levels of TG, TC, Insulin, and BHB were measured using commercial detection kits following the manufacturer's protocols. Hippocampal tissues were homogenized in ice-cold PBS at a 10% (w/v) ratio using a motor-driven homogenizer. The homogenates were centrifuged at 12,000 rpm for 10 min at 4 °C. The resulting supernatant was collected for subsequent analysis of A $\beta$ 40 and A $\beta$ 42 levels.

### Histological analysis

Coronal paraffin-embedded liver sections (4  $\mu$ m thick) were stained with H&E for morphological evaluation. The severity of non-alcoholic steatohepatitis was scored using the NAS, which encompasses steatosis (0–3), lobular inflammation (0–3), and hepatocellular ballooning (0–2). To

quantify lipid deposition, fresh liver tissue embedded in optimal cutting temperature compound was cryosectioned at 8  $\mu\text{m}$  and stained with Oil Red O. Liver fibrosis was assessed via Sirius Red staining. The fibrosis stage was scored on a scale of 0–4. Images were captured, and the percentage of Oil Red O-positive area was quantified using ImageJ software.

For neuronal integrity assessment, paraffin-embedded brain sections (5  $\mu\text{m}$  thick) were subjected to Nissl staining with 0.1% cresyl violet. The number of surviving, morphologically intact neurons in the hippocampal CA1, CA2, CA3, and dentate gyrus (DG) regions was quantified. Additionally, brain sections stained with H&E were used for general morphological assessment to evaluate the overall structural integrity of the neural tissue. All evaluations, including scoring and counting, were carried out under blinded conditions by independent peers.

### Immunofluorescence

For immunofluorescence staining, serial coronal brain sections were incubated with primary antibodies. This was followed by incubation with species-matched secondary antibodies. Nuclei were counterstained with 4',6-diamidino-2-phenylindole (Sigma-Aldrich, #D9542) for 5 min at room temperature. Following image acquisition with a fluorescence microscope at 10x magnification, the mean fluorescence intensity for each slide was quantified using ImageJ software. The antibodies used are detailed in Supplementary Table 1.

### Immunohistochemistry

Paraffin-embedded mouse brain sections were subjected to immunohistochemical staining. Endogenous peroxidase activity was blocked by incubation in 3%  $\text{H}_2\text{O}_2$  at 37 °C for 25 min. Antigen retrieval was subsequently performed using microwave irradiation. Sections were then blocked with 3% bovine serum albumin for 30 min. Primary antibodies were applied to detect target protein expression, with antibody dilutions detailed in Supplementary Table 1. After incubation with HRP-conjugated secondary antibodies, signal visualization was achieved using 3,3'-diaminobenzidine. Finally, sections were counterstained with hematoxylin, dehydrated, cleared, and mounted with a coverslip for bright-field microscopy observation. The Histochemistry score (H-Score) was calculated using the Sai-viewer software. For each slide, five fields of view were selected from corresponding regions at 10x magnification. The H-Score is a semi-quantitative histological scoring method that converts the percentage of positive cells and their staining intensity into a single numerical value, enabling a comprehensive assessment of both staining intensity and prevalence.

### Western blot analysis

Liver and hippocampal tissues were homogenized in RIPA lysis buffer supplemented with PMSF. Protein concentrations were measured using a BCA assay. The lysates were separated on SDS-PAGE gels, transferred to PVDF membranes, and blocked with a quick-sealing solution for 30 min at room temperature. The membranes were incubated with primary antibodies overnight at 4 °C, with antibody dilutions detailed in Supplementary Table 1. Following washing, the membranes were incubated with HRP-conjugated secondary antibodies for 1 h and visualized using ECL reagents (Biosharp Life Sciences, #BL523A).

### Statistics and reproducibility

Statistical processing was carried out via SPSS 26.0, and graph generation was accomplished using GraphPad Prism 8.0. The unpaired Student's *t*-test was employed to evaluate the disparities between two groups, whereas one-way analysis of variance (ANOVA) with Tukey's post-hoc comparison was utilized to assess the differences among multiple groups. A *p*-value < 0.05 was considered to indicate statistical significance. Data are presented as mean  $\pm$  SEM, with all individual data points shown as dots. The 'n' in the figure legend indicates the number of biological replicates from biologically independent samples, and the specific number for each group is provided in the corresponding legend.

### Data availability

All data supporting the findings of this study are available within the paper and its Supplementary Information. Uncropped and unedited blot images are shown in Supplementary Figs. 5–11. Source data for the main figures are provided in Supplementary Data File 1. Additional data are available from the corresponding author upon request.

### Code availability

This paper does not report any new generated original code.

Received: 25 June 2025; Accepted: 30 December 2025;

Published online: 10 January 2026

### References

- Le, M. H. et al. Forecasted 2040 global prevalence of nonalcoholic fatty liver disease using hierarchical Bayesian approach. *Clin. Mol. Hepatol.* **28**, 841–850 (2022).
- Wong, V. W., Ekstedt, M., Wong, G. L. & Hagstrom, H. Changing epidemiology, global trends and implications for outcomes of NAFLD. *J. Hepatol.* **79**, 842–852 (2023).
- Targher, G., Tilg, H. & Byrne, C. D. Non-alcoholic fatty liver disease: a multisystem disease requiring a multidisciplinary and holistic approach. *Lancet Gastroenterol. Hepatol.* **6**, 578–588 (2021).
- Colognesi, M., Gabbia, D. & De Martin, S. Depression and cognitive impairment-extrahepatic manifestations of NAFLD and NASH. *Biomedicines* **8**, E229 (2020).
- Yu, Q. et al. Association between metabolic dysfunction-associated fatty liver disease and cognitive impairment. *J. Clin. Transl. Hepatol.* **10**, 1034–1041 (2022).
- Cushman, M. et al. Nonalcoholic fatty liver disease and cognitive impairment: a prospective cohort study. *PLoS One* **18**, e0282633 (2023).
- Doward, L. C. et al. Development of a patient-reported outcome measure for non-alcoholic steatohepatitis (NASH-CHECK): results of a qualitative study. *Patient* **14**, 533–543 (2021).
- Kennedy-Martin, T., Bae, J. P., Paczkowski, R. & Freeman, E. Health-related quality of life burden of nonalcoholic steatohepatitis: a robust pragmatic literature review. *J. Patient Rep. Outcomes* **2**, 28 (2017).
- Dede, A. J., Wixted, J. T., Hopkins, R. O. & Squire, L. R. Hippocampal damage impairs recognition memory broadly, affecting both parameters in two prominent models of memory. *Proc. Natl. Acad. Sci. USA* **110**, 6577–6582 (2013).
- Gold, S. M. et al. Hippocampal damage and memory impairments as possible early brain complications of type 2 diabetes. *Diabetologia* **50**, 711–719 (2007).
- Cheon, S. Y. & Song, J. Novel insights into non-alcoholic fatty liver disease and dementia: insulin resistance, hyperammonemia, gut dysbiosis, vascular impairment, and inflammation. *Cell Biosci.* **12**, 99 (2022).
- Kaya, E. & Yilmaz, Y. Association of metabolic dysfunction-associated fatty liver disease with cognitive impairment and all-cause dementia: a comprehensive review. *Turk. J. Gastroenterol.* **35**, 76–82 (2024).
- Kim, J. H. et al. Protective effects of krill oil on high fat diet-induced cognitive impairment by regulation of oxidative stress. *Free Radic. Res.* **55**, 799–809 (2021).
- Xu, J. et al. Melatonin alleviates cognition impairment by antagonizing brain insulin resistance in aged rats fed a high-fat diet. *J. Pineal Res.* **67**, e12584 (2019).
- Xu, J. et al. Docosahexaenoic acid enhances hippocampal insulin sensitivity to promote cognitive function of aged rats on a high-fat diet. *J. Adv. Res.* **45**, 31–42 (2023).
- Newman, J. C. & Verdin, E. Beta-hydroxybutyrate: a signaling metabolite. *Annu. Rev. Nutr.* **37**, 51–76 (2017).

17. Croci, I. et al. Whole-body substrate metabolism is associated with disease severity in patients with non-alcoholic fatty liver disease. *Gut* **62**, 1625–1633 (2013).
18. Nasser, S. et al. Ketogenic diet administration to mice after a high-fat-diet regimen promotes weight loss, glycemic normalization and induces adaptations of ketogenic pathways in liver and kidney. *Mol. Metab.* **65**, 101578 (2022).
19. Ohashi, T. et al. Conophylline inhibits high fat diet-induced non-alcoholic fatty liver disease in mice. *PLoS One* **14**, e0210068 (2019).
20. Asif, S. et al. Hmgcs2-mediated ketogenesis modulates high-fat diet-induced hepatosteatosis. *Mol. Metab.* **61**, 101494 (2022).
21. Yan, A. et al. Beta-hydroxybutyrate upregulates FGF21 expression through inhibition of histone deacetylases in hepatocytes. *Open Life Sci.* **17**, 856–864 (2022).
22. Hu, L. T. et al. HMGCS2-induced autophagic degradation of tau involves ketone body and ANKRD24. *J. Alzheimers Dis.* **91**, 407–426 (2023).
23. Wu, Y. et al. BHBA treatment improves cognitive function by targeting pleiotropic mechanisms in transgenic mouse model of Alzheimer's disease. *FASEB J.* **34**, 1412–1429 (2020).
24. Iwanaga, T. & Kishimoto, A. Cellular distributions of monocarboxylate transporters: a review. *Biomed. Res.* **36**, 279–301 (2015).
25. Al Haj Ahmad, R. M., Ababneh, N. A. & Al-Domi, H. A. Brain insulin resistance as a mechanistic mediator links peripheral metabolic disorders with declining cognition. *Diab. Metab. Syndr.* **16**, 102468 (2022).
26. Zheng, M. et al. Research progress on the association of insulin resistance with type 2 diabetes mellitus and Alzheimer's disease. *Metab. Brain Dis.* **40**, 35 (2024).
27. Gao, Z. et al. Butyrate improves insulin sensitivity and increases energy expenditure in mice. *Diabetes* **58**, 1509–1517 (2009).
28. Bae, H. R. et al. Beta-hydroxybutyrate suppresses inflammasome formation by ameliorating endoplasmic reticulum stress via AMPK activation. *Oncotarget* **7**, 66444–66454 (2016).
29. Duda, P. et al. Targeting GSK3 signaling as a potential therapy of neurodegenerative diseases and aging. *Expert Opin. Ther. Targets* **22**, 833–848 (2018).
30. Zhang, L. et al. Colorimetric and surface-enhanced Raman scattering dual-mode magnetic immunosensor for ultrasensitive detection of blood phosphorylated tau in Alzheimer's disease. *Biosens. Bioelectron.* **222**, 114935 (2023).
31. Tang, Z. et al. *Treponema denticola* Induces Alzheimer-like tau hyperphosphorylation by activating hippocampal neuroinflammation in mice. *J. Dent. Res.* **101**, 992–1001 (2022).
32. Chen, X. Q. et al.  $\gamma$ -Secretase modulator BPN15606 reduced A $\beta$ 42 and A $\beta$ 40 and countered alzheimer-related pathologies in a mouse model of down syndrome. *Ann. Neurol.* **96**, 390–404 (2024).
33. De Strooper, B. & Karran, E. New precision medicine avenues to the prevention of Alzheimer's disease from insights into the structure and function of  $\gamma$ -secretases. *Embo J.* **43**, 887–903 (2024).
34. Chen, S. Y., Koch, M., Chávez-Gutiérrez, L. & Zacharias, M. How modulator binding at the amyloid  $\beta$ - $\gamma$ -secretase interface enhances substrate binding and attenuates membrane distortion. *J. Med. Chem.* **66**, 16772–16782 (2023).
35. Kjærgaard, K. et al. Cognitive dysfunction in early experimental metabolic dysfunction-associated steatotic liver disease is associated with systemic inflammation and neuroinflammation. *JHEP Rep.* **6**, 100992 (2024).
36. Zuo, W. et al. CA3 pyramidal neuron activation promotes cognitive resilience to inflammation-induced cognitive inflexibility. *CNS Neurosci. Ther.* **31**, e70271 (2025).
37. Liu, L. & Chan, C. The role of inflammasome in Alzheimer's disease. *Ageing Res. Rev.* **15**, 6–15 (2014).
38. Bomfim, T. R. et al. An anti-diabetes agent protects the mouse brain from defective insulin signaling caused by Alzheimer's disease-associated A $\beta$  oligomers. *J. Clin. Invest.* **122**, 1339–1353 (2012).
39. Gage, M. C. & Thippeswamy, T. Inhibitors of Src family kinases, inducible nitric oxide synthase, and NADPH oxidase as potential CNS drug targets for neurological diseases. *CNS Drugs* **35**, 1–20 (2021).
40. Picca, A. et al. Age-associated glia remodeling and mitochondrial dysfunction in neurodegeneration: antioxidant supplementation as a possible intervention. *Nutrients* **14**, 2406 (2022).
41. Kajitani, N. et al. Prefrontal cortex infusion of beta-hydroxybutyrate, an endogenous NLRP3 inflammasome inhibitor, produces antidepressant-like effects in a rodent model of depression. *Neuropsychopharmacol. Rep.* **40**, 157–165 (2020).
42. Bai, Y. P. et al.  $\beta$ -Hydroxybutyrate suppresses M1 macrophage polarization through  $\beta$ -hydroxybutyrylation of the STAT1 protein. *Cell Death Dis.* **15**, 874 (2024).
43. Cotter, D. G. et al. Ketogenesis prevents diet-induced fatty liver injury and hyperglycemia. *J. Clin. Invest.* **124**, 5175–5190 (2014).
44. d'Avignon, D. A. et al. Hepatic ketogenic insufficiency reprograms hepatic glycogen metabolism and the lipidome. *JCI Insight* **3**, e99762 (2018).
45. Bragoszewski, P., Habor, A., Walewska-Zielecka, B. & Ostrowski, J. Expression of genes encoding mitochondrial proteins can distinguish nonalcoholic steatosis from steatohepatitis. *Acta Biochim. Pol.* **54**, 341–348 (2007).
46. Yang, X. et al. Beta-hydroxybutyrate alleviates learning and memory impairment through the SIRT1 pathway in D-galactose-injured mice. *Front. Pharmacol.* **12**, 751028 (2021).
47. Hu, E. et al. Beta-hydroxybutyrate promotes the expression of bdnf in hippocampal neurons under adequate glucose supply. *Neuroscience* **386**, 315–325 (2018).
48. Youm, Y. H. et al. The ketone metabolite beta-hydroxybutyrate blocks NLRP3 inflammasome-mediated inflammatory disease. *Nat. Med.* **21**, 263–269 (2015).
49. Wang, R. et al.  $\beta$ -Hydroxybutyrate alleviates brain aging through the MTA1 pathway in D-galactose injured mice. *Eur. J. Pharmacol.* **983**, 176959 (2024).

## Acknowledgements

This study was supported by the National Natural Science Foundation of China (grant number 82474318), the Jiangsu Administration of Traditional Chinese Medicine (grant number QN202411), the special fund for training outstanding young doctors in the second session of Jiangsu Province Hospital of Chinese Medicine (grant number 2024QB002), the project funded by Jiangsu Province Hospital of Chinese Medicine (grant number KKZX01), and the Hefei Municipal Health Science and Technology Project (grant number Hwk2025zd017).

## Author contributions

This study was conceptualized and designed by L.N., Q.X., and X.Z. L.N. performed the majority of the experiments, acquired and analyzed the data, and drafted the manuscript. J.S. and W.X. contributed some immunofluorescence and immunohistochemistry experiments, and analyzed some data. X.Y., G.W., and Y.W. assisted in the performance of animal experiments and reproduction of HMGCS2 KO mice. T.J., Y.C., and H.C. contributed to the performance of H&E stainings and immunoblotting. Q.X. revised the manuscript and provided critical feedback. X.Z. supervised the study, had full access to the data, and is responsible for the integrity of the data and accuracy of the analysis. All authors approved the final manuscript.

## Competing interests

The authors declare no competing interests.

## Additional information

**Supplementary information** The online version contains supplementary material available at <https://doi.org/10.1038/s42003-026-09513-1>.

**Correspondence** and requests for materials should be addressed to Qingrong Xia or Xiqiao Zhou.

**Peer review information** *Communications Biology* thanks Norifumi Kawada and the other, anonymous, reviewer(s) for their contribution to the peer review of this work. Primary Handling Editors: Ibrahim Javed and Benjamin Bessieres.

**Reprints and permissions information** is available at <http://www.nature.com/reprints>

**Publisher's note** Springer Nature remains neutral with regard to jurisdictional claims in published maps and institutional affiliations.

**Open Access** This article is licensed under a Creative Commons Attribution-NonCommercial-NoDerivatives 4.0 International License, which permits any non-commercial use, sharing, distribution and reproduction in any medium or format, as long as you give appropriate credit to the original author(s) and the source, provide a link to the Creative Commons licence, and indicate if you modified the licensed material. You do not have permission under this licence to share adapted material derived from this article or parts of it. The images or other third party material in this article are included in the article's Creative Commons licence, unless indicated otherwise in a credit line to the material. If material is not included in the article's Creative Commons licence and your intended use is not permitted by statutory regulation or exceeds the permitted use, you will need to obtain permission directly from the copyright holder. To view a copy of this licence, visit <http://creativecommons.org/licenses/by-nc-nd/4.0/>.

© The Author(s) 2026